Hindawi
Journal of Advanced Transportation
Volume 2017, Article ID 4073583, 11 pages
https://doi.org/10.1155/2017/4073583

Research Article

Modeling Passengers' Boarding Behavior at the Platform of High Speed Railway Station

Tie-Qiao Tang,[1,2] Yi-Xiao Shao,[1] Liang Chen,[1] and Hua-Yan Shang[3]

[1]*School of Transportation Science and Engineering, Beijing Key Laboratory for Cooperative Vehicle Infrastructure Systems and Safety Control, Beihang University, Beijing 100191, China*
[2]*MOE Key Laboratory for Urban Transportation Complex Systems Theory and Technology, Beijing Jiaotong University, Beijing 100044, China*
[3]*Information College, Capital University of Economics and Business, Beijing 100070, China*

Correspondence should be addressed to Tie-Qiao Tang; tieqiaotang@buaa.edu.cn

Received 27 May 2017; Revised 28 August 2017; Accepted 2 October 2017; Published 31 October 2017

Academic Editor: Zhi-Chun Li

Modeling passengers' motion at high speed railway (HSR) station has been a hot topic in the field of pedestrian flow theory. However, little effort has been made to explore the passengers' boarding behaviors at the platform of HSR station. This study proposes a cellular automaton (CA) model to study the passengers' boarding behavior at the platform of HSR station. Some numerical tests are conducted to explore the passengers' movements and the complex traffic phenomena (e.g., each passenger's trajectory, congestion, and travel time) which occur during the boarding process. The numerical results illustrate that the passengers' inflow rate and entrance choice behavior have significant impacts on the boarding efficiency. These results can help managers to understand the passengers' boarding behavior and to improve the boarding efficiency.

1. Introduction

With the rapid development of urbanization, overcrowding occurs in many stations, stadiums, and other public places [1, 2]. For example, most stations (metro ones, railway ones, etc.) experience extremely high level of pedestrian density during the peak hours and often produce serious traffic problems (e.g., congestion and accident) [3–5], which has attracted many researchers to explore the complex traffic phenomena produced by the pedestrian flow at the traffic stations [6–8].

High speed railway (HSR) has been considered as a significant technological breakthrough of transportation tool in the 20th century [9], so HSR and its stations have been built in many countries [10]. With the rapid development of HSR, the HSR passenger volume sharply increases (especially in China) [11] and many traffic problems have occurred [12]. The traffic problems have attracted researchers' attention, where the studies can be sorted into social impact [13–15], safety [16, 17], and operational management [18–20].

However, the studies [13–20] do not belong to the field of pedestrian flow and cannot be used to explore the complex phenomena produced by the pedestrian flow at HSR station. In fact, few researchers studied the pedestrian flow at the HSR stations, but some models were proposed to study the pedestrian flow at the conventional railway station and metro station. For example, Wang et al. [21] simulated the pedestrian flow in the hall of conventional railway station during the Spring Festival travel rush and found that casualties happened when passengers escaped from panic induced by crowd turbulence and that the number of passengers, the ticket checking patterns, the baggage volumes, and the passengers' anxiety can all affect the speed of passing through the waiting corridor. Jiang et al. [22] used the software building EXODUS and field observation to explore the crowding at a platform staircase of a subway station in China and found that the simulation software can be applied to assess the flow rate and the evacuation capacity of public places by adjusting the staircase width and the maximum upstairs walking speed. Based on

Table 1: Comparison of railway, subway and HSR station platform.

	Layout		Management	Pedestrian characteristic		
	Entrance	Obstacle	Seat/carriage allocation	Density	Direction	Boarding\alighting behavior
Railway station	One entrance (see Figure 1(a))	No obstacle	Beforehand allocated	Relatively low	Bidirectional or unidirectional	Boarding or alighting
Metro station	Two or more entrances (see Figure 1(b))	The entrances are obstacles	Self-determined options	Relatively high	Bidirectional	Boarding and alighting simultaneously
HSR station	Two entrances (see Figure 1(c))	The entrances are obstacles	Beforehand allocated	Relatively low	Unidirectional	Boarding

observations of passenger alighting and boarding behavior and field data, Zhang et al. [23] proposed a cellular automata-based alighting and boarding microsimulation model for passengers in Beijing metro stations to explore the components of the alighting and boarding time and the effects of different group sizes on the alighting and boarding performances. The results proved that the proposed model can reproduce the fundamental features of alighting and boarding movement. To propose criteria for pedestrian traffic management at the platform and doors of metro cars, Seriani and Fernandez [24] used a pedestrian traffic microsimulator and experiments to study the effects of pedestrian traffic management on the pedestrian's boarding/alighting time at metro station and found that the pedestrian traffic management has significant impacts on the passenger Level of Service (LOS), Passenger Service Time (PST), passenger density in cars and at platform, and passengers' dissatisfaction in metro station. Duduta and Subedi [25] studied passenger overcrowding in a bus rapid transit station and obtained a pedestrian capacity range for a BRT station and the quantitative impacts of friction between pedestrians entering and leaving the station.

However, the scenarios in [21–25] are not the HSR station, so the studies [21–25] cannot be used to study the pedestrian flow at HSR station. In fact, HSR stations and the scenarios in [21–25] have some common characteristics (e.g., the boarding behavior, congestion), so the studies [21–25] can be extended to explore the pedestrian flow at HSR station.

During the boarding process at HSR station, platform and hall are two important scenarios. To study this topic, Tang et al. [26] proposed a cellular automaton (CA) model to investigate the passenger flow in the hall of HSR station during the check-in process and found that the passengers' arrival rate in the hall and the service efficiency of ticket barrier have significant effects on the passengers' movements and the efficiency with which the passengers run across the ticket barrier, but they did not further explore the passengers' movements at the platform of HSR station.

At the platform of HSR stations, pedestrian movements are different from those at the platforms of other stations due to the platform layout and passenger management. Currently, each HSR platform is equipped with two entrances. Also, the entrances are regarded as obstacles for those who move at the platform. Passenger seats are allocated beforehand; thus the destination carriage is allocated as well. In terms of pedestrian flow, the density is relatively low at HSR platform. Pedestrian flow in an origin HSR station is unidirectional flow and correspondingly boarding behavior is the significant pedestrian characteristic. The comparison of railway, subway, and HSR station platform in terms of layout, management, and pedestrian characteristics is summarized in Table 1.

Specifically, the pedestrian movements at the platform of HSR stations have the following three attributes: (1) the pedestrian flow on a HSR platform is usually of low density and is close to a free flow since the platform size of HSR station is greater than that of other stations (i.e., the length is usually several hundred meters and the width is more than ten meters), that is, the congestion only occurs around the entrance and near the carriage's door. (2) The HSR platform is always equipped with two entrances (see Figure 1(c)). One ticket gate approaches an entrance at the platform (i.e., two ticket gates serve for a platform in the meantime). Passengers have to choose one of the two ticket gates to enter the platform. It is ordinary for passengers to choose appropriate ticket gate and entrances (i.e., passengers are informed which ticket gate should be chosen on the tickets before checking in). Choosing an improper ticket gate and entrance cannot be ignored. Thus, the entrance choice behavior has some impacts on the passengers' movements at platform and is worth investigating as well. (3) Each passenger's seat is allocated beforehand, so he has to move to the destination carriage rather than any other available carriage, which is similar to conventional railway but differs from metro railway. Therefore, the pedestrian flow at HSR platform may consist of branch flows.

2. Model

Pedestrian flow models can roughly be sorted into macroscopic ones and microscopic ones. The macroscopic models explore the macroscopic features of pedestrian flow (e.g., speed, density, and flow), where the fluid dynamic model [29, 30] is a well-known macroscopic model. The fluid dynamic model [29, 30] can describe the pedestrian collective movements, where the results are qualitatively accordant with those observed in real situations (e.g., the development of walking lane, jam, the propagation of wave, and the behavior on a dance floor) [29]. The microscopic models study the

(a) Layout of platform of railway station in [27]

(b) Layout of platform of metro station in [28]

(c) Layout of platform of HSR station

Figure 1: Architectural structure of platform of different stations.

pedestrian individual motion and the related complex phenomena and can be sorted into continuous ones [31–33] and discrete ones [34–46]. One of the typical continuous models is the social force model [31–33]. The discrete models can be sorted into lattice-gas models [34–37] and CA models [38–46]. The lattice-gas models were, respectively, used to study the jamming transition in pedestrian counterflow at the free moving state (e.g., low density) and the stopped state (e.g., high density) [34]. Later, researchers extended the work [34] and developed some extended lattice-gas model for pedestrian flow [35–37]. As for the CA model for pedestrian flow, Burstedde et al. [38] and Blue and Adler [39] firstly used CA model to explore pedestrian flow, where the scenarios were uniformly divided into cells and each pedestrian moved to his neighboring cell or stay at his current cell at each time step. Later, researchers extended the studies [38, 39] to study the bidirection pedestrian flow [40], the exit and route choice behaviors [41–43], and the competitive and cooperative behaviors [44, 45].

In this paper, a CA model is used to study the passengers' movements at the platform of HSR station, where the scenario is equally divided into cells and the Moore neighborhood is used to update each passenger's movement at each time step. Each pedestrian at cell m, k has nine options since this cell has eight neighboring cells (see Figure 2), where each option's transition probability is completely determined by the nine cells' potentials. For simplicity, the logit model is used here to define the transition probability; that is,

$$P_{m,k}^{i,j} = \frac{N_{i,j}}{\sum_{c=m-1}^{m+1} \sum_{d=k-1}^{k+1} N_{c,d}}, \quad i \in [m-1, m+1]; \; j \in [k-1, k+1], \tag{1}$$

where $P_{m,k}^{i,j}$ is the transition probability that the passenger at cell m, k chooses cell i, j; $N_{i,j}$ is the potential of cell i, j. Thus, the numerator is the potential of cell i, j, the denominator is the sum of the nine cells' potentials in the Moore neighborhood, and the sum of the transition probabilities is equal to 1.

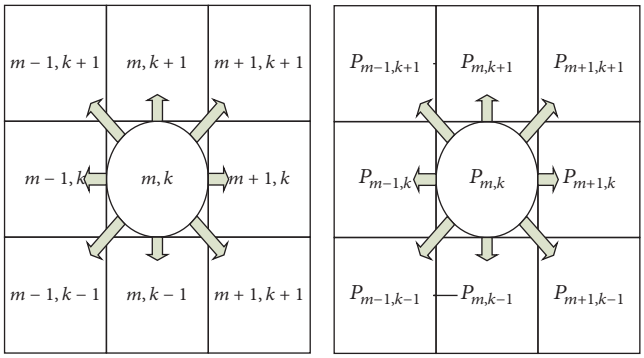

Figure 2: The scheme of Moore's neighborhood.

$N_{i,j}$ is relevant to the static floor field potential and dynamic potential of cell i, j, so it can simply be defined as follows:

$$N_{i,j} = E_{i,j} \exp\left(k_S S_{i,j} + k_D D_{i,j}\right), \tag{2}$$

where $S_{i,j}$, $D_{i,j}$ are, respectively, the static floor field potential and dynamic potential of cell i, j; k_S, k_D are two corresponding parameters; $E_{i,j}$ is a 0-1 variable that can be defined as follows:

$$E_{i,j} = \begin{cases} 1, & \text{if the cell is empty} \\ 0, & \text{if the cell is occupied or obstacle.} \end{cases} \tag{3}$$

$S_{i,j}$ is static potential and determined by the destination's attraction and obstacles' repulsion, so it can be defined as the weighted sum of $L_{i,j}$ and $O_{i,j}$; that is,

$$S_{i,j} = k_L L_{i,j} + k_O O_{i,j}, \tag{4}$$

where $L_{i,j}$ is geometry distance between the cell i, j and the destination; $O_{i,j}$ is the obstacle repulsion on pedestrian

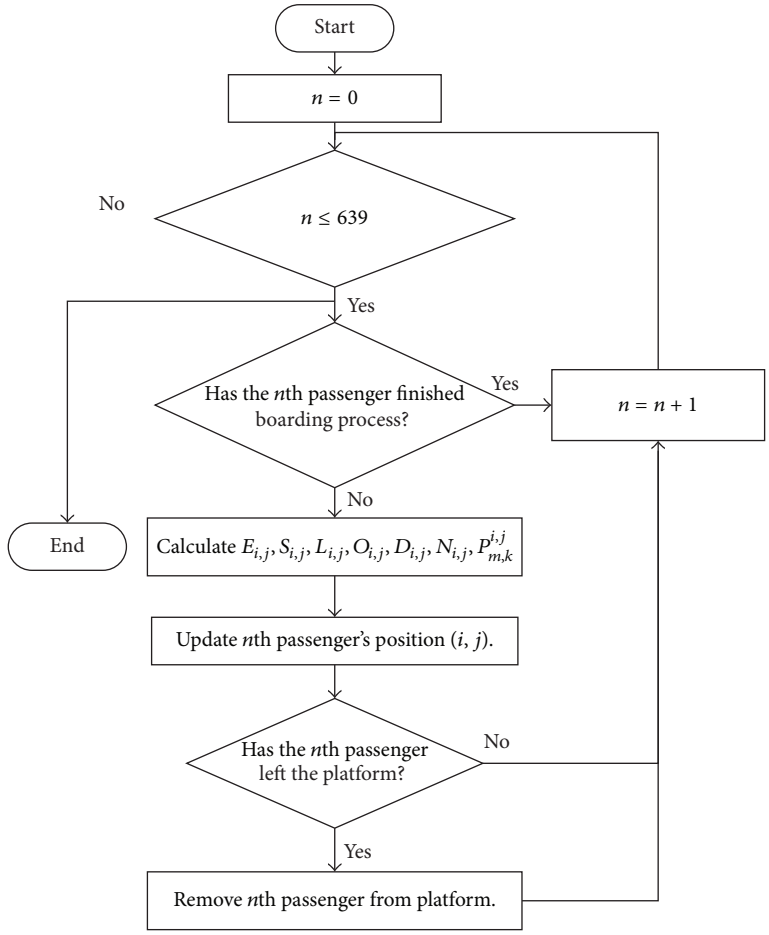

Figure 3: The flow chart of update rules at each time step.

movement and defined as the number of cells that are not an obstacle cell among the eight neighboring cells of cell i, j; k_L, k_O are two corresponding parameters.

Since $D_{i,j}$ is determined by the attraction between the two adjacent passengers and the repulsions among the congested crowds, congestion degree can be used to define $D_{i,j}$, where $D_{i,j}$ denotes the number of empty cells among the eight neighboring cells of cell i, j.

For simplicity, (2) and (4) can be incorporated; that is,

$$N_{i,j} = E_{i,j} \exp\left(k_1 L_{i,j} + k_2 O_{i,j} + k_3 D_{i,j}\right). \quad (5)$$

$N_{i,j}$ drops with $L_{i,j}$ and increases with $O_{i,j}$, $D_{i,j}$, so $k_1 < 0$, $k_2 > 0$, $k_3 > 0$. The three parameters have no qualitative effects on the simulation results and the quantitative effects of k_1, k_2, k_3 on pedestrian movement are hard to obtain and beyond the scope of this paper, so the three parameters can be defined as follows:

$$\begin{aligned} k_1 &= -5, \\ k_2 &= 1, \\ k_3 &= 1. \end{aligned} \quad (6)$$

Based on the above discussion, the passengers' motion update rules at each time step are summarized in the flow chart shown in Figure 3.

This model is developed from the basic CA model. And it is possible that the simulation results of this model can be realized by other models.

3. Simulation

In this section, the proposed model is used to explore each passenger's boarding behavior at the platform of HSR station. To display the feature of each passenger's movement, it is necessary to introduce the scenario of the platform at HSR station and give some basic assumptions in advance.

3.1. Scenario and Assumptions. At the platform of HSR station, passengers' movements can simply be formulated as follows.

(1) Passengers enter the platform from two entrances and will choose the entrance that is close to their target carriage.

(2) The density near each entrance at the platform is relatively high. The two entrances are located in the middle of the platform, so the passenger flow can be divided into two parts, where some passengers go ahead and others go back.

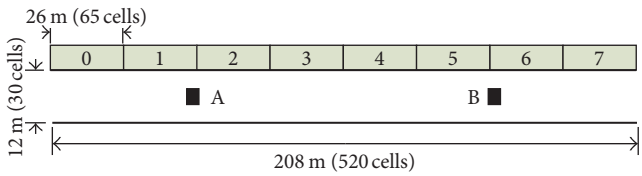

Figure 4: The simplified sketch of the HRS platform.

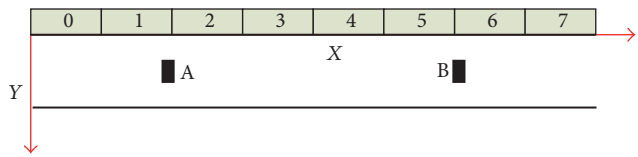

Figure 5: Definition of x axis and y axis.

At this time, the passenger flow in this area may be somewhat chaotic.

(3) After leaving the high-density area, most passengers move in free flow and walk in a straight line along the carriage until they arrive at the door of their target carriage.

(4) When reaching the target carriage, passengers immediately enter the carriage since the ticket checking is always ignored at the platform of the HSR station.

Before simulation, we should give the following assumptions based on field observations.

(1) The platform is defined as a rectangle with 208 m length and 12 m width (see Figure 4). 208 m is a HSR train's length that is shorter than length of a real platform. Because passengers only appear in the range of a train length, the platform length can be set as 208 m for simplicity.

(2) The platform is uniformly divided into $520 * 30$ cells, where each cell's size is $0.4\,\text{m} * 0.4\,\text{m}$; each entrance's size is $10 * 10$ cells; the length of carriage is 65 cells; the width of a carriage door is 1 cell, which means that passengers cannot enter the carriage side by side.

(3) Each passenger's initial position lies at the right hand of square A or the left hand of square B (here, A and B denote two entrances and their sizes are $10 * 10$ cells), where each passenger selects the entrance closer to his target carriage (see Figure 4).

(4) The number of passengers is 640; each passenger's desired speed is 1 m/s; each carriage contains 80 passengers; the time step is 0.4 s.

(5) The average check-time of passengers at each ticker barrier is set as 12 time steps based on [26], and 8 ticket barriers are used, so the average time headway at the platform is 1.5 time step (i.e., a passenger enters the platform within 1.5 time steps). According to this assumption, it can be obtained that each entrance's average inflow rate at the platform is 3000 passengers in an hour.

3.2. Simulation Results. First, this study explores each passenger's trajectory at the platform of HSR station during the boarding process. If a one-dimensional curve is used to describe each passenger's trajectory at the platform during the boarding process, some prominent features of the trajectory curves cannot be summarized since the curves are relatively chaotic. Therefore, each passenger's trajectory is placed in the X- or Y-direction to study the features. At this time, the platform is set as Figure 5, where the coordinates of A and B in the X-direction are, respectively, 121–130 cells and 391–400 cells, and those of B in the Y-direction are 12–21 cells.

Figure 6 shows each passenger's trajectory in the X-Y plane. From this figure, the following findings can be summarized.

(1) In the X-direction, all passengers enter the platform continuously from the two entrances. The trajectories are sorted into two parts without overlap (i.e., the up curves correspond to the trajectories of the passengers entering the platform from the right hand of entrance A and the down ones correspond to the trajectories of the passengers entering the platform from the left hand of entrance B) since all passengers are assumed to select the entrance closer to their target carriage at the platform. The above numerical results are shown in Figure 6(a).

(2) The passengers who have the same target carriages have similar trajectories in the X-direction and the tested HSR train has eight carriages, so the curves in the X-direction can be separated into eight groups, where each group corresponds to the trajectories of the passengers with the same target carriage. At this time, curves I–VIII, respectively, correspond to the trajectories of the passengers whose target carriages are the 0–7 carriages (see Figure 6(a)).

(3) Most curves in curves I, II, IV, V, VI, and VIII are approximately smooth straight lines; that is, most passengers' speeds in the X-direction are approximately constant, where the reasons can be formulated as follows: (i) these passengers' destinations are the same, (ii) their movements in the X-direction are very similar, and (iii) their distances in the X-direction are much larger than the ones in the Y-direction (see Figure 6(a)).

(4) In the Y-direction, each passenger moves from his initial position to $y = 1$. Ten horizontal lines occur, which shows that each passenger's initial position is within [12, 21] and that most passengers straightly move ahead to avoid the congestion near each entrance. During the early stage of the boarding process, when the passengers enter the platform from A or B, some passengers are pushed to the positions whose Y-values are larger than 21, but their Y-values will finally be 1. In a word, the trajectories are relatively disorder in the Y-direction. All the above numerical results are shown in Figure 6(b).

Figure 6 shows that congestion occurs (especially in the Y-direction) at the platform during the boarding process, so we next study the features of the congestion. At a wide platform, congestion does not occur frequently during the boarding process, so "push and bump" rarely takes place; even if congestion happens, it is weak and cannot cause "push and bump." However, how the density of crowd is distributed at the platform and what impacts the degree of congestion has on the crowd density have been two important topics. To

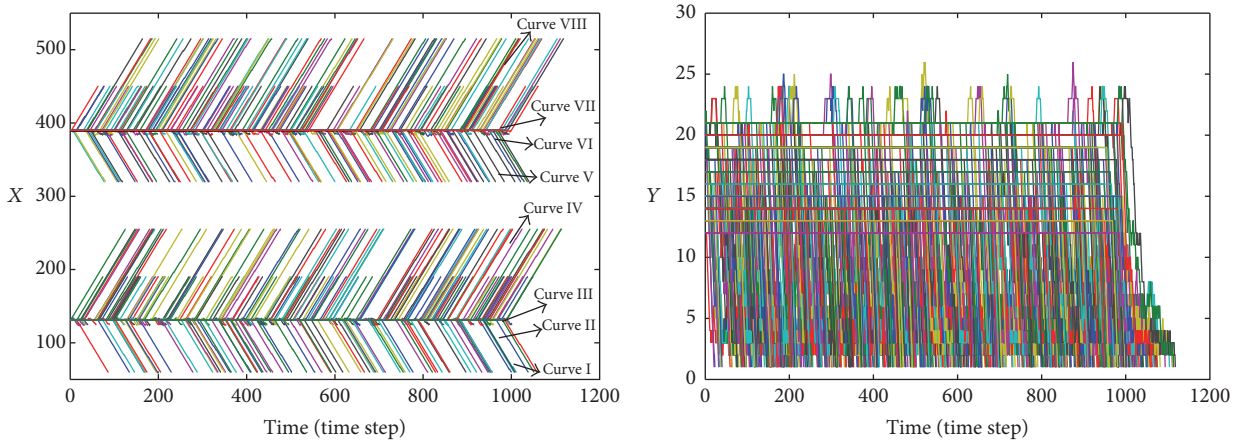

Figure 6: Each pedestrian's trajectory, where (a) is the x-direction and (b) is the y-direction.

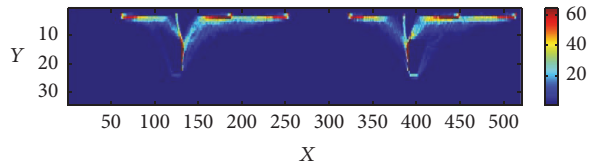

Figure 7: $CD_{i,j}$ during the boarding process.

Table 2: The relationships between the number of cells with high cumulative density and total inflow rate.

Total inflow rate	$CD_{ij} \geq 40$	$CD_{ij} \geq 50$	$CD_{ij} \geq 60$
4500	275.5	172.9	93.9
6000	274	167.3	90.7
9000	264.3	163.5	81.6

understand the passenger density distribution, it is necessary to define the cumulative density of a cell as follows:

$$CD_{i,j} = \sum_{t=1}^{ST} \delta_{i,j}^{t}, \tag{7}$$

where $CD_{i,j}$ is the cumulative density of cell i, j, t is the tth time step, ST is the total number of time steps of a simulation, $\delta_{i,j}^{t}$ is a 0-1 variable that can be defined as follows:

$$\delta_{i,j}^{t} = \begin{cases} 1, & \text{if cell } i, j \text{ is occupied at } t \\ 0, & \text{otherwise.} \end{cases} \tag{8}$$

According to (7), it is not hard to calculate $CD_{i,j}$ at the platform of HSR station during the boarding process (see Figure 7). From Figure 7, the following findings are summarized as follows.

(1) Frequently occupied cells are placed near each entrance and spread to the door of each carriage along the correspond route, so $CD_{i,j}$ near each entrance and each door are both relatively high.

(2) The passengers with the same carriage select the routes near the path to this carriage door, so $CD_{i,j}$ near this path are relatively high.

(3) During the boarding process, some passengers occur below A or B; that is, their Y-values are slightly larger than 20 and they should bypass A or B since $CD_{i,j}$ near A or B is relatively high.

The cumulative density of cells can quantitatively reflect the spatial distribution of passengers during the boarding process. The total inflow rate decides the density around the path. Thus how the inflow rate affects the spatial distribution is to be studied. Table 2 presents results of the number of cells with high cumulative density in different total inflow rate by repeatedly simulations. Some conclusions and explanations are given.

(1) The number of cells with high cumulative density drops with the increase of the total inflow rate. The reasons are as follows: (a) the higher total inflow rate means that more passengers appear at the platform simultaneously, and an individual has to occupy the space of 0.4 m $*$ 0.4 m at least (both in reality and in our model). Thus a wider path (more cells are selected and used) is generated. And the sum of all passengers' travel times is almost a constant (it can be got by the results of Figure 7 easily). So the average cumulative density of these high cumulative density cells drops, and the number of cells with high cumulative density decreases consequently. (b) The lower total inflow rate means that fewer passengers appear at the platform simultaneously. Thus a narrower path is generated. And the sum of all passengers' travel times is almost a constant. So the average cumulative density of the path cells increases, and the number of cells with high cumulative density increases consequently.

(2) When the cumulative density increases, the number of cells with high cumulative density prominently drops, where the reason is obvious.

Table 2 shows that the total inflow rate has impacts on the cumulative density. The average arrival interval is the only parameter that determines the total inflow rate, so this parameter affects the passengers' movements at the platform

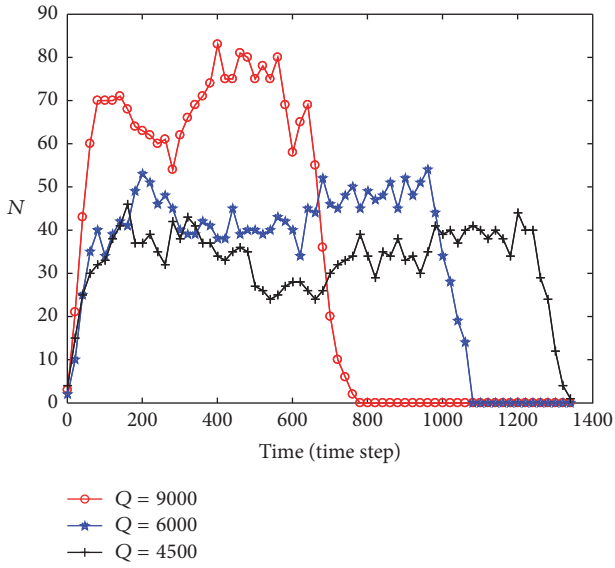

FIGURE 8: The relationships between N and Q during the boarding process, where Q is the total inflow rate and N is the number of passengers at the platform.

during the boarding process. Next, this study explores the effects of the average arrival interval on the passengers' movements at the platform during the boarding process. The average arrival interval is set as 1.5 time steps, and it is set as 1.0 time step and 2.0 time steps as comparison. To display the effects of the total inflow rate (Q) on the passengers' movements, it is reasonable to transform the average arrival interval into the total inflow rate, that is, when the average arrival intervals are 1.0 time step, 1.5 time steps, and 2.0 time steps, the total inflow rates are, respectively, 9000 ped/hour, 6000 ped/hour, and 4500 ped/hour. Likely, it is easy to calculate the number of passengers (N) at the platform during the boarding process (see Figure 8). From this figure, the following findings are obtained.

(1) N has similar changing trend under the three total inflow rates; that is, during the boarding process, N first rapidly increases and then becomes relatively stable but produces slight oscillation and finally sharply drops to zero.

(2) Q influences the maximum value of N and the time step when the maximum value occurs. When Q is 9000 ped/hour, more passengers simultaneously enter the platform and quickly scatter at the platform, so the maximum of N is relatively high but the boarding process is quickly over. When Q is 4500 ped/hour, fewer passengers simultaneously enter the platform, so the maximum of N is relatively small, the passenger crowd does not reach the capacity of the carriage door (i.e., congestion does not occur), and the boarding process is relatively long. The above results show that the maximum of N increases while the boarding process is lessened with the increase of Q.

Each passenger's travel time at the platform is an important factor of boarding efficiency, so it is needed to study it. Here, each passenger's travel time at the platform is defined as the difference between the time that he leaves the platform and the time that he enters the platform. To eliminate the randomness, the average travel time of passengers is defined; that is,

$$T_{\text{average}} = \frac{1}{n}\sum_{i=1}^{n}\left(t_i - t_{i,0}\right), \tag{9}$$

where T_{average} is the average travel time of passengers at the platform; t_i is the time when the ith passenger leaves the platform; $t_{i,0}$ is the time when the ith passenger enters the platform; n is the number of passengers. For convenience, T is utilized to represent each passenger's travel time at the platform. Note that the unit of T, T_{average} is time step.

The passengers with different carriages have different route and the distances between their origins and destinations are different and directly affect T, T_{average}, so the relationships between T, T_{average}, and D (D is the length of each passenger's route and its unit is cell) are studied, where the numerical results are shown in Figure 9. The following is shown.

(1) T is separately divided into groups I, II, III, and IV, where T in groups I–IV, respectively, is in $[10, 23]$, $[58, 73]$ $[69, 88]$, and $[123, 146]$. The four groups correspond to the travel time of the passengers whose carriage is C1/C5, C6/C2, C0/C4, and C7/C3 (C0–C7 are the carriage number). The quantitative relationship between T and D can be fitted by a linear function; that is,

$$T = 1.0388 * D - 2.6996, \tag{10}$$

where $R^2 = 0.9946$ is the correlation efficient. Equation (10) indicates that T is completely determined by D and increases with D.

(2) The quantitative relationship between T_{average} and D can be fitted by a linear function; that is,

$$T_{\text{average}} = 1.0385 * D - 2.6779, \tag{11}$$

where $R^2 = 0.9986$ is the correlation efficient. Equation (11) shows that T_{average} is also completely determined by D and increases with D.

To better understand the distribution features of T, Figure 10 provides SD_T (standard deviation) and RSD_T (relative standard deviation). From Figure 10, the following findings can be concluded:

(1) There are no prominent relationships between SD_T and D.

(2) The relationships between RSD_T and D are prominent and can well be fitted by a quadratic polynomial; that is,

$$\text{RSD}_T = 0.0029 * D^2 - 0.59 * D + 30, \tag{12}$$

where $R^2 = 0.9783$ is the correlation efficient. From Figure 10, it can be found that the travel time of the passengers whose carriages are C1/C5 has larger relative standard deviation than that of the passengers with other carriages, where the reason is that the travel time of the passengers in C1/C5 has relatively large standard deviation but extremely small mean value.

The passenger's travel time can be used to qualitatively evaluate the boarding efficiency, but it is not intuitionistic and

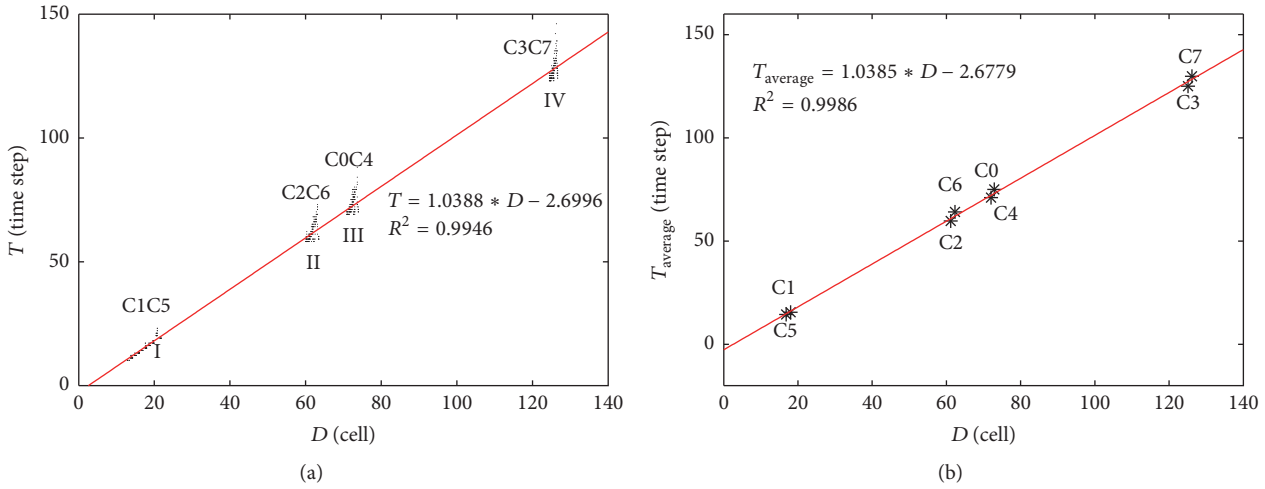

FIGURE 9: The relationships between T, T_{average}, and D, where (a) is T and (b) is T_{average}.

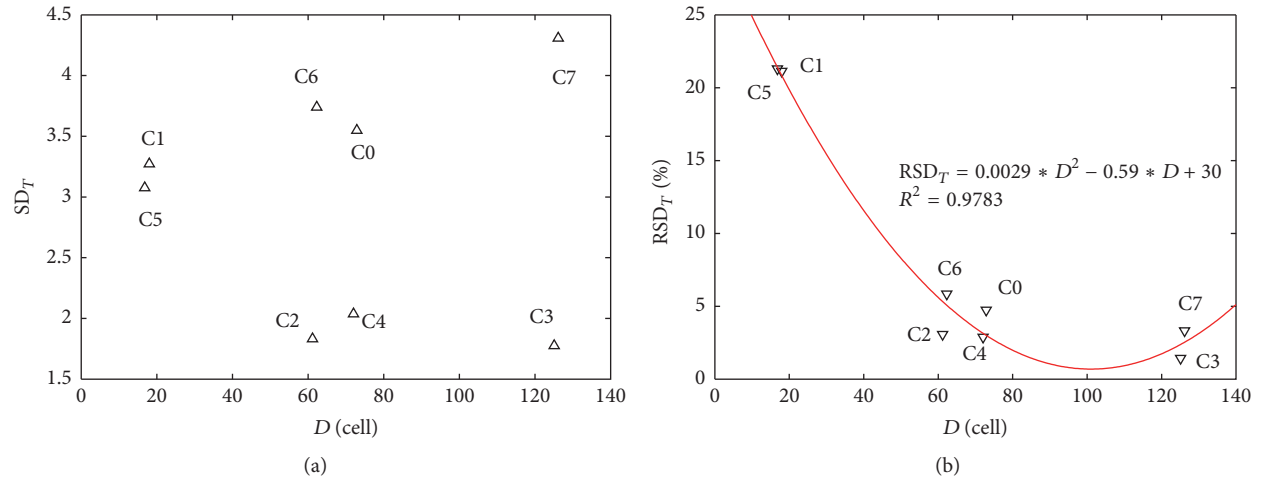

FIGURE 10: The relationship between SD_T, RSD_T, and D, where (a) is SD_T and (b) is RSD_T.

cannot provide his real route. The passenger's real route may be longer than the distance between his initial position and target carriage during the boarding process, so the passenger's real route can be used to evaluate the boarding efficiency. An index is defined to study the boarding efficiency; that is,

$$\eta_i = \frac{\sum_{j=1}^{N_i} \rho_{i,j}}{N_i}, \quad i = 0, 1, 2, 3, 4, 5, 6, 7, \tag{13}$$

where η_i is the passengers' average movement efficiency in Ci; $\rho_{i,j}$ is the movement efficiency of the jth passenger in Ci; N_i is the number of passengers whose carriage is Ci. Here, $\rho_{i,j}$ can be defined as follows:

$$\rho_{i,j} = \frac{D_{i,j}}{\text{PL}_{i,j}}, \tag{14}$$

where $D_{i,j}$ is the distance between Ci and the jth passenger in Ci; $\text{PL}_{i,j}$ is the length of the real route of the jth passenger in Ci. Note that $0 < \eta_i, \rho_{i,j} \leq 1$.

Equation (14) shows that η_i can reflect the extent that the passengers' real routes in Ci deviate from the shortest ones between their initial positions and Ci; that is, when η_i increases, the passengers' real routes become close to their shortest ones in Ci. Based on the above discussions, η_i during the boarding process can be calculated easily (see Figure 11). It can be found that $\eta_i \in [0.77, 0.84]$, $\eta_1 > \eta_i$ $(i = 0, 2, 3)$, and $\eta_5 > \eta_i$ $(i = 4, 6, 7)$, where the detailed results can be formulated as follows.

(1) The routes from A (B) to C1 (C5) are similar to a straight line. At this time, the passengers whose target carriage is C1 (C5) move along the straight lane, so the passengers' average movement efficiency is very high. As for the passengers whose destinations are other carriages, they

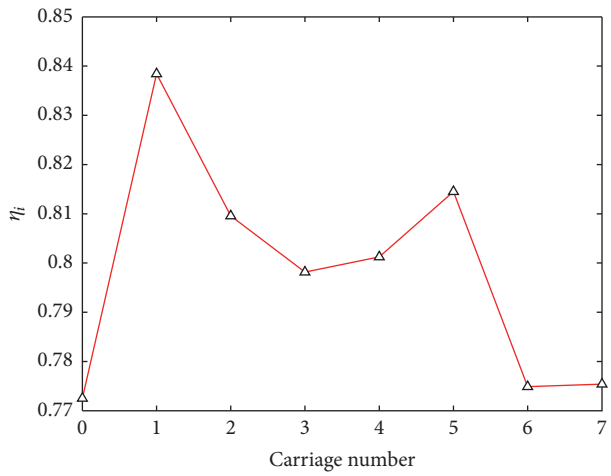

Figure 11: The passengers' average movement efficiency of each carriage.

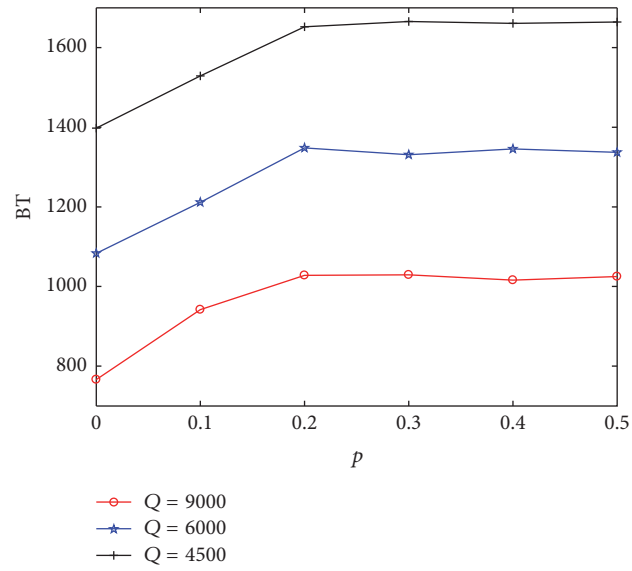

Figure 12: The boarding time under different Q.

have to make a turn when they enter the platform, so the real routes may deviate from the shortest route between their initial positions and target carriages; that is, the passengers' average movement efficiency is relatively low.

(2) The trajectories of the passengers whose destination is C1 (C5) do not almost interweave with those of other passengers, so the passengers in C1 (C5) are not distributed in a wide area during the boarding process. This is another reason that makes the average movement efficiency of the passengers in C1 (C5).

In the above numerical tests, all passengers are assumed to select the entrance close to their carriage. However, some passengers may select the entrance far away from their carriage, where the passengers' percentage is set as p. In this paper, $p \in [0, 0.5]$ and $p = 0$ means that each passenger selects the entrance close to his carriage. Since the boarding time (that is equal to the difference between the time when the last passenger leaves the platform and the time when the first passenger enters the platform) and the cumulative density are influenced by p, we explore the impacts. Figure 12 displays the BT-p curve (BT is the boarding time) under different Q, and Figure 13 displays $CD_{i,j}$ under different p when $Q = 6000$.

From Figure 12, the following can be concluded.

(1) When $p \leq 0.2$, BT gradually increases with p. This shows that p is an important factor that influences BT when p is very small.

(2) When $p > 0.2$, BT is approximately a constant. This shows that p has no prominent impacts on BT when p is relatively high.

(3) BT drops with the increase of Q. This shows that Q is always an important factor that influences BT.

From Figure 13, the following can be concluded.

(1) Some interweaving between passengers occurs at the middle of the platform.

(2) The amount of interweaving increases with p. In the interweaving area, counterflow occurs. It is very hard for some passengers to move in the counterflow, which will reduce the boarding efficiency.

4. Conclusion

In this paper, a CA model is used to study each passenger's movement at the platform of HSR station during the boarding process. In this CA model, the static floor field potential and dynamic potential are calculated to update passenger movements. The simulation results display several indexes (i.e., trajectories, congestion, travel time, and movement efficiency), which shows that the proposed model can perfectly describe each passenger's movement at the platform during the boarding process. Finally, the numerical results show that the parameter p has significant impacts on BT and $CD_{i,j}$.

Comparing with the existing studies, this study has the following new insights: (1) the simulation results show that passenger movements at platform are significantly influenced by their destination carriage; (2) passengers' entrance choice behavior (which rarely draws researchers' attention) is studied and the results show that the improper choice will not only produce bidirectional flow, but also prolong boarding time.

However, this paper still has the following limitations:

(1) Only the parameter Q is obtained by the field observed data and other parameters are not calibrated by empirical or experimental data.

(2) The simulation results are not testified by experimental or video data.

(3) The simulation conditions used in this paper are not calibrated by the pedestrians' attributes at the platform.

Therefore, experimental/empirical data are going to be used to propose a more realistic boarding model for HSR station and study various complex phenomena occurring during the HSR boarding process.

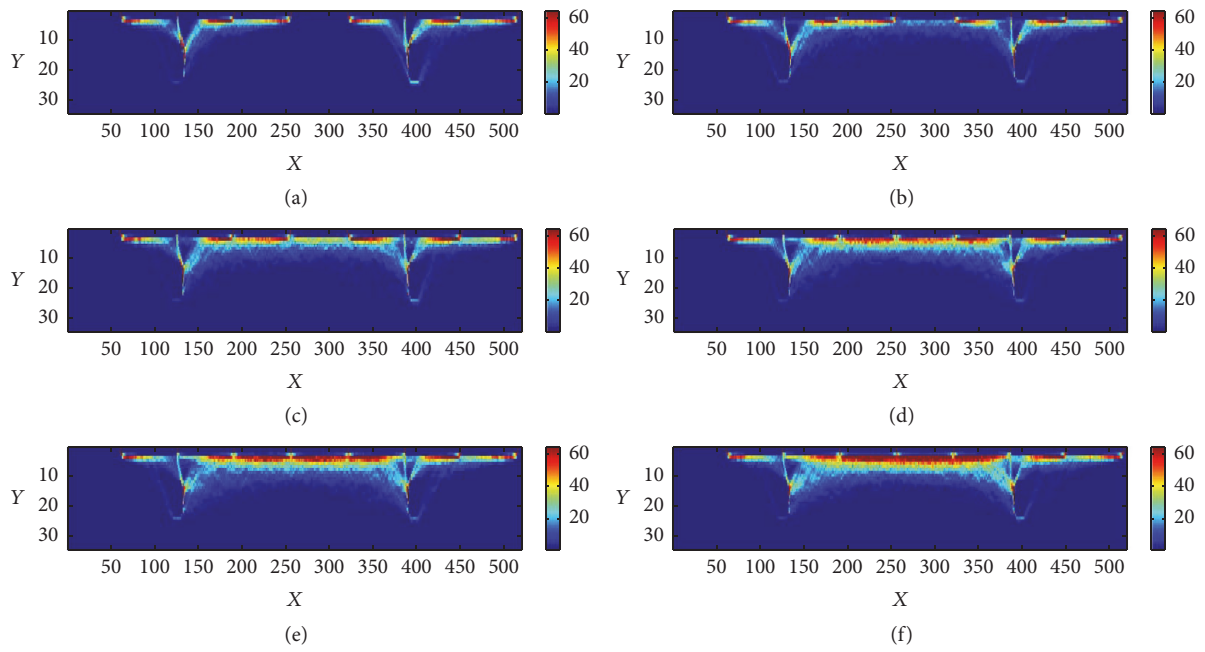

FIGURE 13: $CD_{i,j}$ under different p, where p in (a)–(f) are, respectively, 0, 0.1, 0.2, 0.3, 0.4, and 0.5.

Conflicts of Interest

The authors declare that they have no conflicts of interest.

Acknowledgments

This work was supported by the National Natural Science Foundation of China (71771005, 71422001, and 71371128) and the Foundation of MOE Key Laboratory for Urban Transportation Complex Systems Theory and Technology in Beijing Jiaotong University.

References

[1] J. Li, L. Wang, S. Tang, B. Zhang, and Y. Zhang, "Risk-based crowd massing early warning approach for public places: A case study in China," *Safety Science*, vol. 89, pp. 114–128, 2016.

[2] S. Wang, R. Zhou, and L. Zhao, "Forecasting Beijing transportation hub areas's pedestrian flow using modular neural network," *Discrete Dynamics in Nature and Society*, vol. 2015, Article ID 749181, 2015.

[3] X. Wang, J. Yang, C. Lee, Z. Ji, and S. You, "Macro-level safety analysis of pedestrian crashes in Shanghai, China," *Accident Analysis & Prevention*, vol. 96, pp. 12–21, 2016.

[4] J. Wang, L. Zhang, Q. Shi, P. Yang, and X. Hu, "Modeling and simulating for congestion pedestrian evacuation with panic," *Physica A: Statistical Mechanics and its Applications*, vol. 428, pp. 396–409, 2015.

[5] J. V. D. Heuvel, A. Voskamp, W. Daamen, and S. P. Hoogendoorn, "Using bluetooth to estimate the impact of congestion on pedestrian route choice at train station," *Traffic and Granular Flow*, pp. 73–82, 2015.

[6] J. Xu, Y. Ning, H. Wei et al., "Route choice in subway station during morning peak hours: A case of Guangzhou subway," *Discrete Dynamics in Nature and Society*, vol. 2015, Article ID 151434, 2015.

[7] X. Ji, J. Zhang, Y. Hu, and B. Ran, "Pedestrian movement analysis in transfer station corridor: Velocity-based and acceleration-based," *Physica A: Statistical Mechanics and its Applications*, vol. 450, pp. 416–434, 2016.

[8] R. Thoreau, C. Holloway, G. Bansal, K. Gharatya, T.-R. Roan, and N. Tyler, "Train design features affecting boarding and alighting of passengers," *Journal of Advanced Transportation*, vol. 50, no. 8, pp. 2077–2088, 2016.

[9] J. Campos and G. De Rus, "Some stylized facts about high-speed rail: a review of HSR experiences around the world," *Transport Policy*, vol. 16, no. 1, pp. 19–28, 2009.

[10] A. Ryder, "High speed rail," *Journal of Transport Geography*, vol. 22, pp. 303–305, 2012.

[11] K. Takagi, "Development of high-speed railways in China," *Japan Railway and Transport Review*, vol. 57, pp. 36–41, 2011.

[12] M. Janić, "A multidimensional examination of performances of HSR (High-Speed Rail) systems," *Journal of Modern Transportation*, vol. 24, no. 1, pp. 1–21, 2016.

[13] D. M. Levinson, "Accessibility impacts of high-speed rail," *Journal of Transport Geography*, vol. 22, pp. 288–291, 2012.

[14] S. Masson and R. Petiot, "Can the high speed rail reinforce tourism attractiveness? The case of the high speed rail between Perpignan (France) and Barcelona (Spain)," *Technovation*, vol. 29, no. 9, pp. 611–617, 2009.

[15] G. He, A. P. J. Mol, and Y. Lu, "Public protests against the Beijing-Shenyang high-speed railway in China," *Transportation Research Part D: Transport and Environment*, vol. 43, pp. 1–16, 2016.

[16] M. Guo, W. Wei, G. Liao, and F. Chu, "The impact of personality on driving safety among Chinese high-speed railway drivers," *Accident Analysis & Prevention*, vol. 92, pp. 9–14, 2016.

[17] X. Jin, X. Xiao, L. Ling, L. Zhou, and J. Xiong, "Study on safety boundary for high-speed train running in severe environments," *International Journal of Rail Transportation*, vol. 1, no. 1-2, pp. 87–108, 2013.

[18] T. W. Chiang, H. Y. Hau, H. M. Chiang, S. Y. Ko, and C. H. Hsieh, "Knowledge-based system for railway scheduling," *Data Knowledge Engineering*, vol. 27, p. 289, 1998.

[19] Y.-C. Lai, M.-C. Shih, and G.-H. Chen, "Development of efficient stop planning optimization process for high-speed rail systems," *Journal of Advanced Transportation*, vol. 50, no. 8, pp. 1802–1819, 2016.

[20] Y. Yue, S. Wang, L. Zhou, L. Tong, and M. R. Saat, "Optimizing train stopping patterns and schedules for high-speed passenger rail corridors," *Transportation Research Part C: Emerging Technologies*, vol. 63, pp. 126–146, 2016.

[21] L. Wang, Q. Zhang, Y. Cai, J. Zhang, and Q. Ma, "Simulation study of pedestrian flow in a station hall during the Spring Festival travel rush," *Physica A: Statistical Mechanics and its Applications*, vol. 392, no. 10, pp. 2470–2478, 2013.

[22] C. S. Jiang, Y. F. Deng, C. Hu, H. Ding, and W. K. Chow, "Crowding in platform staircases of a subway station in China during rush hours," *Safety Science*, vol. 47, no. 7, pp. 931–938, 2009.

[23] Q. Zhang, B. Han, and D. Li, "Modeling and simulation of passenger alighting and boarding movement in Beijing metro stations," *Transportation Research Part C: Emerging Technologies*, vol. 16, no. 5, pp. 635–649, 2008.

[24] S. Seriani and R. Fernandez, "Pedestrian traffic management of boarding and alighting in metro stations," *Transportation Research Part C: Emerging Technologies*, vol. 53, pp. 76–92, 2015.

[25] N. Duduta and A. Subedi, "Understanding platform overcrowding at bus rapid transit stations," *Transportation Research Record*, vol. 2533, pp. 118–123, 2015.

[26] T.-Q. Tang, Y.-X. Shao, and L. Chen, "Modeling pedestrian movement at the hall of high-speed railway station during the check-in process," *Physica A: Statistical Mechanics and its Applications*, vol. 467, pp. 157–166, 2017.

[27] M. Davidich, F. Geiss, H. G. Mayer, A. Pfaffinger, and C. Royer, "Waiting zones for realistic modelling of pedestrian dynamics: a case study using two major German railway stations as examples," *Transportation Research Part C: Emerging Technologies*, vol. 37, pp. 210–222, 2014.

[28] H. W. Yao, Q. E. Wang, Z. Zhao, Y. P. Zheng, and D. Liang, "Pedestrian flow characteristics in different union of metro station," *Journal of Residuals Science Technology*, vol. 13, 2016.

[29] D. Helbing, "A fluid-dynamic model for the movement of pedestrians," *Complex Systems*, vol. 6, no. 5, pp. 391–415, 1992.

[30] L. F. Henderson, "On the fluid mechanics of human crowd motion," *Transportation Research*, vol. 8, no. 6, pp. 509–515, 1974.

[31] D. Helbing, "A mathematical model for the behavior of pedestrians," *Behavioural Science*, vol. 36, no. 4, pp. 298–310, 1991.

[32] D. Helbing and P. Molnár, "Social force model for pedestrian dynamics," *Physical Review E: Statistical, Nonlinear, and Soft Matter Physics*, vol. 51, no. 5, pp. 4282–4286, 1995.

[33] A. Johansson, D. Helbing, and P. K. Shukla, "Specification of the social force pedestrian model by evolutionary adjustment to video tracking data," *Advances in Complex Systems. A Multidisciplinary Journal*, vol. 10, no. suppl. 2, pp. 271–288, 2007.

[34] M. Muramatsu, T. Irie, and T. Nagatani, "Jamming transition in pedestrian counter flow," *Physica A: Statistical Mechanics and its Applications*, vol. 267, no. 3-4, pp. 487–498, 1999.

[35] D. Helbing, M. Isobe, T. Nagatani, and K. Takimoto, "Lattice gas simulation of experimentally studied evacuation dynamics," *Physical Review E: Statistical, Nonlinear, and Soft Matter Physics*, vol. 67, no. 6, Article ID 067101, p. 067101/4, 2003.

[36] Y. Tajima and T. Nagatani, "Scaling behavior of crowd flow outside a hall," *Physica A: Statistical Mechanics and its Applications*, vol. 292, no. 1-4, pp. 545–554, 2001.

[37] R. Jiang and Q.-S. Wu, "Pedestrian behaviors in a lattice gas model with large maximum velocity," *Physica A: Statistical Mechanics and its Applications*, vol. 373, pp. 683–693, 2007.

[38] C. Burstedde, K. Klauck, A. Schadschneider, and J. Zittartz, "Simulation of pedestrian dynamics using a two-dimensional cellular automaton," *Physica A: Statistical Mechanics and its Applications*, vol. 295, no. 3-4, pp. 507–525, 2001.

[39] V. J. Blue and J. L. Adler, "Cellular automata microsimulation for modeling bi-directional pedestrian walkways," *Transportation Research Part B: Methodological*, vol. 35, no. 3, pp. 293–312, 2001.

[40] J. Li, L. Z. Yang, and D. L. Zhao, "Simulation of bi-direction pedestrian movement in corridor," *Physica A*, vol. 354, pp. 619–628, 2005.

[41] A. Varas, M. D. Cornejo, D. Mainemer et al., "Cellular automaton model for evacuation process with obstacles," *Physica A: Statistical Mechanics and its Applications*, vol. 382, no. 2, pp. 631–642, 2007.

[42] H. J. Huang and R. Y. Guo, "Static floor field and exit choice for pedestrian evacuation in rooms with internal obstacles and multiple exits," *Physical Review E: Statistical, Nonlinear, and Soft Matter Physics*, vol. 78, no. 2, Article ID 021131, 6 pages, 2008.

[43] R.-Y. Guo, H.-J. Huang, and S. C. Wong, "Route choice in pedestrian evacuation under conditions of good and zero visibility: Experimental and simulation results," *Transportation Research Part B: Methodological*, vol. 46, no. 6, pp. 669–686, 2012.

[44] A. Kirchner, H. Klupfel, K. Nishinari, A. Schadschneider, and M. Schreckenberg, "Simulation of competitive egress behavior: comparison with aircraft evacuation data," *Physica A: Statistical Mechanics and its Applications*, vol. 324, no. 3-4, pp. 689–697, 2003.

[45] L. Z. Yang, D. L. Zhao, J. Li, and T. Y. Fang, "Simulation of the kin behavior in building occupant evacuation based on Cellular Automaton," *Building and Environment*, vol. 40, no. 3, pp. 411–415, 2005.

[46] K. Yamamoto, S. Kokubo, and K. Nishinari, "Simulation for pedestrian dynamics by real-coded cellular automata (RCA)," *Physica A: Statistical Mechanics and its Applications*, vol. 379, no. 2, pp. 654–660, 2007.